Available online at www.sciencedirect.com
ScienceDirect
Trans. Nonferrous Met. Soc. China 35(2025) 1662−1678
Transactions of Nonferrous Metals Society of China
www.tnmsc.cn

Interfacial adsorption and reactivity of exact separation of sphalerite and pyrite by ferrophilic inhibitors in EX−Cu(II) system

Wen-chao DONG, Run-qing LIU, Chang-tao WANG, Zheng-qiang CAO, Wei SUN

School of Minerals Processing and Bioengineering, Central South University, Changsha 410083, China

Received 24 August 2023; accepted 27 February 2024

Abstract: Tetrasodium iminodisuccinate (IDS) was used as an inhibitor in the separation of sphalerite and pyrite in the EX−Cu(II) (ethyl xanthate and Cu^{2+}) system. The flotation test results demonstrated that IDS can effectively separate sphalerite and pyrite under low alkaline conditions. Furthermore, high-quality zinc concentrates with a Zn grade of 58.48% and a recovery of 91.24% through mixed mineral flotation were obtained. The fundamental mechanisms were investigated through surface wettability tests, adsorption capacity tests, LEIS, FTIR, and XPS. The results confirmed that IDS prevents the adsorption of EX on the surface of pyrite, thereby reducing the response and reactivity of pyrite. The introduction of IDS causes the detachment of Cu^{2+} from the Cu-activated pyrite surface. This process allowed IDS to chelate with the Fe sites on the surface of pyrite through the —COO— and N-centered active groups. By contrast, IDS exhibits weaker adhesion on the surface of Cu-activated sphalerite, making it easily displaced by EX through competitive adsorption.

Key words: interfacial adsorption; reactivity; separation; sphalerite; pyrite; tetrasodium iminodisuccinate

1 Introduction

Zinc metal and its alloys are essential raw materials in various fields such as steel, machinery, electrical, chemical, military, and pharmaceutical industries [1,2]. Zinc mainly comes from sphalerite [3,4], which is commonly associated with polymetallic sulfides such as chalcopyrite, galena, pyrite, and pyrrhotite [5,6]. The exact separation of high-quality sphalerite from pyrite has always been a research hotspot and technological challenge in sulfide ore flotation [7−9]. Given the excellent floatability of pyrite, it easily mixes with zinc concentrate, resulting in excessive sulfur content and affecting the quality of the zinc concentrate [10]. In addition, the smelting of high-sulfur zinc concentrate emits a large amount of sulfur dioxide gas, leading to atmospheric pollution [11,12]. Therefore, the exact separation of sphalerite from pyrite using highly selective pyrite inhibitors holds significant economic and environmental value.

Researchers have conducted extensive research on pyrite inhibitors in froth flotation [13,14]. In industrial applications, the high-alkaline lime process is commonly used to inhibit pyrite [9,15]. Lime hydrolysis produces a large amount of OH^- that can form a hydrophilic film on the surface of pyrite, thereby achieving the desired pyrite inhibition effect. Lime is favored by various mines because of its abundant availability and low cost. However, as ore properties become increasingly complex, issues such as poor selectivity, high dosage, and high transportation costs associated with lime have become more prominent. The extensive use of lime leads to pipeline blockages and difficulties in the wastewater treatment and contradicts the current global advocacy of the

Corresponding author: Run-qing LIU, Tel: +86-13875851194, E-mail: liurunqing@126.com
https://doi.org/10.1016/S1003-6326(25)66774-4

"dual-carbon goal".

Certain inorganic salt oxidizing agents in flotation plants are widely used, including sodium sulfide, sulfite and its salts, H_2O_2, calcium hypochlorite, Fenton reagent and ferrate [10,16−20]. Although these agents can effectively inhibit pyrite in polymetallic sulfide flotation, they pose potential hazards to the atmosphere and soil environment. In recent years, organic inhibitors have been extensively developed, such as dextrin, carboxymethyl cellulose, chitosan, 2-mercaptobenzimidazole, salicylic acid, and tannic acid [21−26]. FENG et al [27] achieved excellent inhibition results through pre-oxidation to enhance the environmentally friendly organic depressant locust bean gum while reducing the reagent dosage. Although researchers have extensively investigated different organic inhibitors for pyrite, their application remains a challenge because of economic and environmental issues.

Tetrasodium iminodisucinate (IDS) belongs to a green and environmentally friendly chelating agent, and it is widely used in water treatment, agriculture, metal corrosion inhibition, and descaling [28,29]. IDS is inexpensive, non-toxic, environmentally friendly, and easily degradable, and it has chelating properties for iron ions. IDS is innovatively applied in the flotation separation of sphalerite and pyrite. Moreover, IDS may be used as an effective agent for the inhibition of pyrite in low-alkalinity environments in practical applications. The performance of IDS as a pyrite inhibitor was investigated through the flotation test in the EX−Cu(II) (ethyl xanthate and Cu^{2+}) system. The fundamental mechanisms underlying the exact separation of sphalerite and pyrite by IDS were comprehensively explored through surface wettability test, adsorption capacity test, localized electrochemical impedance spectroscopy (LEIS), Fourier-transform infrared spectroscopy (FTIR), and X-ray photoelectron spectroscopy (XPS).

2 Experimental

2.1 Minerals and reagents

The natural sphalerite and pyrite used in the experiment were obtained from Yunnan Province, China. Some block-shaped samples were manually selected for the surface wettability and LEIS tests, whereas the others were uniformly crushed and graded. Each level of samples was sealed using a vacuum sealing machine. The particles with sizes ranging from 0.038 to 0.074 mm were used for single and mixed mineral flotation. In addition, the particles with size 0.038 mm were used for XRD, FTIR, UV, and XPS measurements. Chemical composition analysis shows that the Zn content in sphalerite was 65.29 wt.%, and the S content in pyrite was 51.59 wt.%. The purity of sphalerite and pyrite reached 95.30% and 96.70%, respectively.

The XRD patterns of sphalerite and pyrite are shown in Fig. 1. The XRD analysis results indicate few impurities in the two samples, making them suitable for experimentation and mechanism analysis.

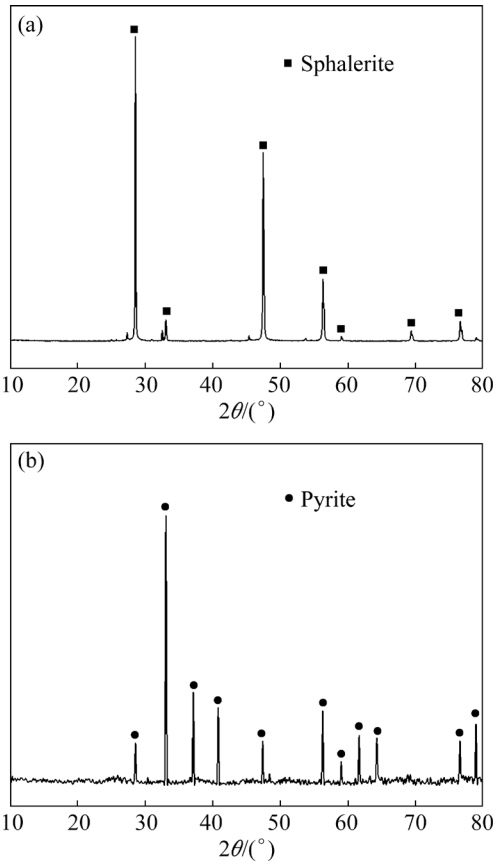

Fig. 1 XRD patterns of sphalerite (a) and pyrite (b)

IDS was used as an inhibitor for pyrite, and its molecular structure is shown in Fig. 2. $CuSO_4$ was used as an activator. EX was used as a collector. NaOH and HCl were used as pH regulators. These reagents were analytically pure and purchased from Sinopharm Chemical Reagent Co., Ltd. The collector was supplied by Hunan Mingzhu Beneficiation Reagent Co., Ltd. Deionized water was used with a resistivity of 18.5 mΩ·cm in all tests.

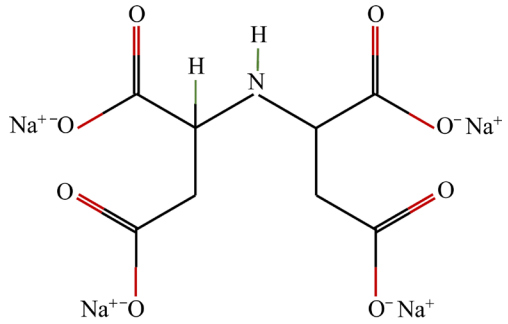

Fig. 2 Molecular structure of IDS

2.2 Micro-flotation tests

Single mineral tests were conducted by using an XFG−1600 flotation machine (Exploring Machinery Plant, Changchun, China). The pulp volume and impeller speed were set to be 40 mL and 1660 r/min, respectively. For each test, 2 g of pure mineral was weighed and placed in an ultrasonic bath for 5 min to be cleaned. The pH value of the pulp was adjusted using HCl or NaOH solution, and then $CuSO_4$ was added to activate the mineral for 3 min. The inhibitor IDS was added if necessary, and the reaction time was 3 min. Subsequently, the collector EX and the frother methyl isobutyl carbinol (MIBC) were added sequentially, with 2 min and 1 min treatment time, respectively. Finally, the froth and tailings were separated, dehydrated, dried, and weighed. The flotation flow chart is shown in Fig. 3. The recovery of the single mineral flotation experiment was calculated using Eq. (1):

$$\varepsilon=\frac{m_1}{m_1+m_2}\times 100\% \tag{1}$$

where ε represents the flotation recovery (%); m_1 and m_2 are the concentrate mass and tailing product mass (g), respectively.

The mixed flotation sample was prepared by mixing sphalerite and pyrite in a mass ratio of 1:1. The mixed mineral flotation test was conducted under the same conditions as the single mineral flotation test. After weighing and assaying the grade of Zn and S, the flotation recoveries of sphalerite and pyrite were then calculated using Eq. (2):

$$\varepsilon=\frac{m_1\cdot\alpha_1}{m_1\cdot\alpha_1+m_2\cdot\alpha_2}\times 100\% \tag{2}$$

where α_1 and α_2 indicate the grades of the concentrate and tailing product (%), respectively.

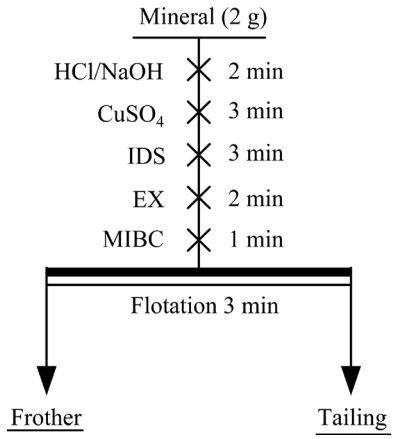

Fig. 3 Scheme of mineral flotation tests

2.3 Surface wettability tests

The surface wettability of sphalerite and pyrite was investigated using a contact angle measuring instrument (JC2000, Shanghai Zhongchen Digital Technology Equipment Co., Ltd., China). Before the measurement, the block sample was polished with a 5000# sandpaper to obtain a smooth mineral surface. Then, the mineral surface was treated with the corresponding reagent and dried using nitrogen gas. Finally, the sample was placed on the test table for contact angle measurement. The sessile drop technique was used for contact angle measurement. Three measurements were taken for each group of tests, and the average value was obtained as the result.

2.4 Reagent adsorption tests

In reagent adsorption analysis, UV−Vis spectrophotometers (UV−2700) were used to quantitatively characterize the effect of IDS on the affinity of EX on sphalerite and pyrite surfaces. The samples were prepared as follows: 2 g of pure mineral with a particle size <0.038 mm was cleaned for 5 min in an ultrasonic bath, and then 40 mL of deionized water was added to the sample before being placed on a constant-temperature magnetic stirrer. Following the flotation test reagent system, reagents were sequentially added. After the reaction was completed, the pulp was filtered and centrifuged. Finally, the supernatant was taken for the reagent adsorption test.

The calculation formula of adsorption capacity is expressed by Eq. (3):

$$\Gamma_{\mathrm{M}}=\frac{(C_0-C)\cdot V}{m} \tag{3}$$

where Γ_M (mol/g) indicates the adsorption capacity of EX; C_0 (mol/L) and C (mol/L) are the initial and final concentrations of EX, respectively; V (L) and m (g) refer to the volume of the solution and the mass of the sample, respectively.

2.5 LEIS tests

LEIS was used in the electrochemical workstation (Versa SCAN, AMETEK Inc, USA). A three-electrode system was used in this test, with Ag/AgCl serving as the reference electrode, the sample as the working electrode, and a platinum ring as the counter electrode.

The block sample (10 mm × 10 mm × 3 mm) was placed into a mold with a diameter of 3 cm and fixed with solid acrylic glue, and the samples were polished with an abrasive paper and diamond flannelette. Before the test, the samples were ultrasonically cleaned for 5 min. Immediately after cleaning, the samples were placed in a sample cell containing a conductive solution of 1 mmol/L KCl. During the test process, the positioning controller moved the probe to a position 50 μm (±5 μm) above the sample. The test parameters were as follows: a scanning range of 400 μm × 400 μm, a step size of 20 μm, a scanning frequency of 1 kHz, and a fixed experimental voltage of 10 mV. The test procedure is shown in Fig. 4.

2.6 FTIR measurements

The FTIR spectra of Cu-activated sphalerite and pyrite before and after treatment were recorded via FTIR spectrophotometry (Bruker Alpha, Thermo, USA). The sample for the test was prepared as follows: 1 g of pure mineral sample with a particle size <0.038 mm was ultrasonically cleaned for 5 min. Then, 40 mL of deionized water was added to the mineral, and the corresponding reagents were added to the pulp in accordance with the flotation test and stirred for 30 min. After stirring, the pulp was filtered and vacuum dried. The prepared mineral was mixed with KBr at a mass ratio of 1:100 for the test, and the test sample for FTIR was obtained through tableting.

2.7 XPS measurements

The XPS data of chalcopyrite and arsenopyrite were recorded by using a K-Alpha 1063 spectrometer (Thermos Scientific Co., USA). The preparation method of XPS measurement samples was the same as that of FTIR. The parameters of the monochromatic Al K_α X-ray source were 12 kV and 6 mA. Thermo Advantage 5.96 was used to fit and analyze XPS peaks, and all spectra were calibrated using C 1 s at 284.8 eV.

3 Results and discussion

3.1 Micro-flotation results

3.1.1 Single mineral flotation

The impact of Cu^{2+} concentration on the flotation of sphalerite and pyrite was investigated through single mineral tests in the EX−Cu(II) system. As shown in Fig. 5, when Cu^{2+} was not added, the flotation recovery of sphalerite was only around 58%, whereas the recovery of pyrite was

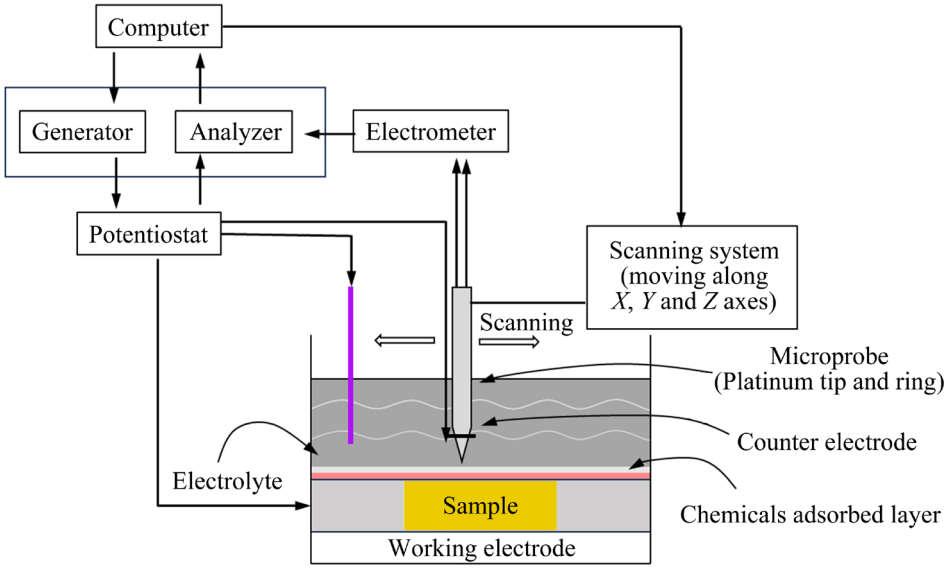

Fig. 4 Flow chart of LEIS test

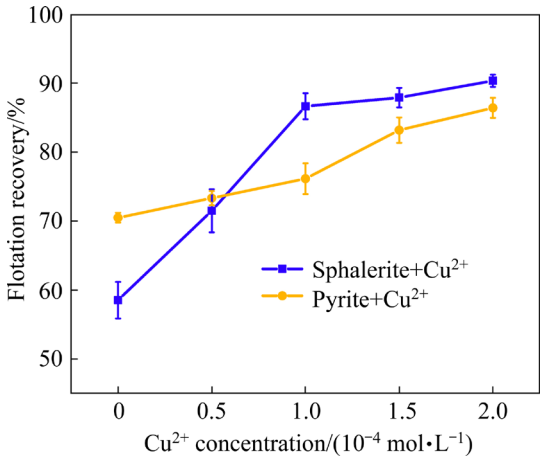

Fig. 5 Effect of Cu^{2+} concentration on flotation recovery of both minerals at pH 8 and EX concentration of 1×10^{-5} mol/L

higher than that of sphalerite, reaching approximately 70%. With the increase of Cu^{2+} concentration, the hydrophobicity of sphalerite markedly increases. When the Cu^{2+} concentration reaches 1×10^{-4} mol/L, the recovery of sphalerite increases to approximately 87%. Further increasing the Cu^{2+} concentration results in a slight improvement in sphalerite recovery. For pyrite, as the Cu^{2+} concentration increases, pyrite recovery shows a steady upward trend. In general, Cu^{2+} has an activating effect on sphalerite and pyrite, with Cu^{2+} showing a stronger activating effect on sphalerite than that on pyrite.

The effects of pH and IDS dosage on the flotation behavior of sphalerite and pyrite in the EX−Cu(II) system were investigated through single mineral flotation. Figure 6 depicts the impact of pH and IDS on the flotation of sphalerite and pyrite in the EX−Cu(II) system. Sphalerite and pyrite demonstrated good floatability in the absence of IDS. The difference in flotation recovery between sphalerite and pyrite remained within 15% in the pH range of 2−10. This result indicates that separating sphalerite from pyrite in the EX−Cu(II) system is difficult when an inhibitor is not added.

After adding 300 mg/L of IDS, significant changes were observed in the flotation behavior of pyrite, with a decrease in its recovery to around 13% at pH 8. The recovery of pyrite only slightly decreased as the pH of the slurry increased further. Throughout the pH range, the recovery of sphalerite only slightly decreased, with a trend almost identical to that observed without adding IDS. After adding IDS, the recovery difference between sphalerite and pyrite reached 70% at pH 8.

Figure 7 illustrates the effect of IDS dosage on the flotation of sphalerite and pyrite in the EX−Cu(II) system. Given the high sensitivity of pyrite to IDS, the recovery of pyrite decreased from 80% to 5.5% when the IDS dosage increased from 0 to 500 mg/L, indicating a strong inhibition of pyrite flotation. As for sphalerite, the recovery remained above 80% when the IDS dosage was between 0 and 300 mg/L but decreased to 70% when the IDS dosage reached 500 mg/L. Therefore, when the IDS dosage was 300 mg/L, the difference in flotation recovery between sphalerite and pyrite was nearly 70%. Therefore, IDS has a significant effect in the flotation separation of sphalerite and pyrite in the EX−Cu(II) system.

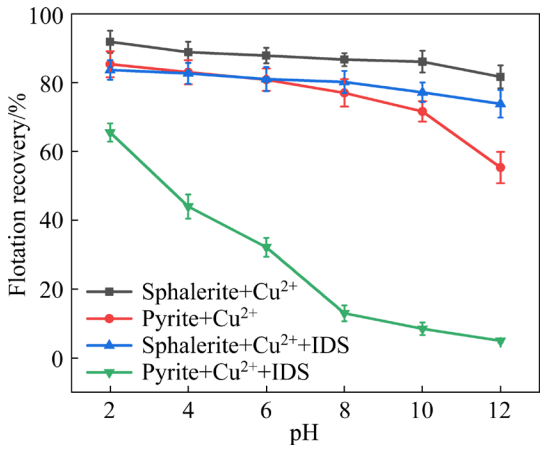

Fig. 6 Flotation performance of both minerals as function of pH at EX concentration of 1×10^{-5} mol/L, Cu^{2+} concentration of 1×10^{-4} mol/L, and IDS dosage of 300 mg/L

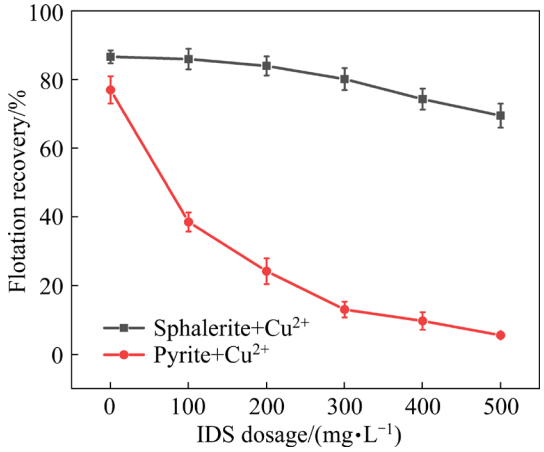

Fig. 7 Effect of IDS dosage on flotation recovery of both minerals at pH 8, EX concentration of 1×10^{-5} mol/L, and Cu^{2+} concentration of 1×10^{-4} mol/L

3.1.2 Mixed mineral flotation

The influence of IDS dosage on the flotation performance of sphalerite and pyrite was investigated in the EX−Cu(II) system through mixed mineral flotation, and the results are shown in Table 1. As the dosage of IDS increased, the Zn grade gradually increased in the concentrate because of the significant inhibitory effect of IDS on pyrite. The increase in IDS dosage led to a sharp decrease in pyrite while having little effect on sphalerite in the concentrate. When the IDS dosage was 300 mg/L, high-quality zinc concentrate with Zn grade and recovery of 58.48% and 91.24%, as well as S grade and recovery of 25.06% and 30.31%, respectively, was obtained. This result demonstrates that IDS can efficiently separate sphalerite and pyrite during mixed mineral flotation.

3.2 Surface wettability

In investigating the mechanism of IDS in the EX−Cu(II) system, the surface wettability of sphalerite and pyrite before and after treatment with IDS was analyzed, as shown in Fig. 8. The contact angle of Cu-activated pyrite was 78.54°, indicating the strong hydrophobicity of Cu-activated pyrite surface. After the addition of IDS, the contact angle of Cu-activated pyrite decreased to 51.28°, which indicated that IDS was attached to the surface of Cu-activated pyrite, increasing its hydrophilicity. After adding EX, the contact angle of the Cu-activated pyrite surface was 54.95° (Fig. 8(a_3)).

Table 1 Mixed mineral flotation results at pH 8, EX concentration of 1×10^{-5} mol/L, and Cu^{2+} concentration of 1×10^{-4} mol/L

IDS dosage/ (mg·L^{-1})	Sample	Yield/%	Grade/%		Recovery/%	
			Zn	S	Zn	S
0	Concentrate	84.79	36.17	36.55	94.30	73.52
	Tailings	15.21	12.18	73.36	5.70	26.48
	Raw ore	100.00	32.52	42.15	100.00	100.00
300	Concentrate	51.16	58.48	25.06	91.24	30.31
	Tailings	48.84	5.88	60.34	8.76	69.69
	Raw ore	100.00	32.79	42.29	100.00	100.00
600	Concentrate	40.72	60.27	21.92	76.03	21.32
	Tailings	59.28	13.05	55.57	23.97	78.68
	Raw ore	100.00	32.28	41.87	100.00	100.00

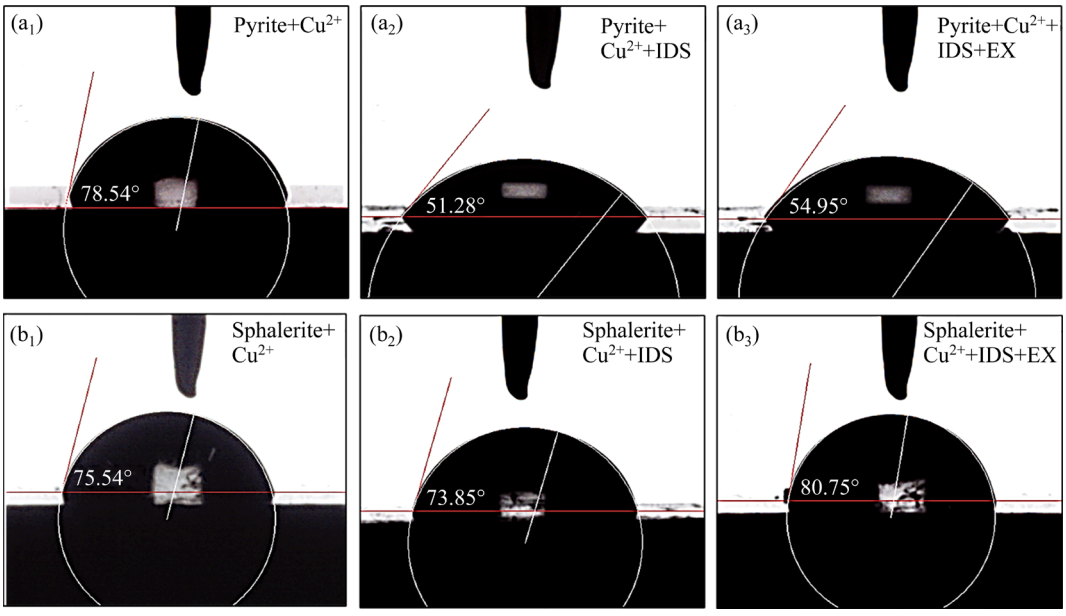

Fig. 8 Contact angles of pyrite and sphalerite

This result indicates that the IDS maintains a high-intensity suppression performance on pyrite in the EX−Cu system.

The contact angle of Cu-activated sphalerite was 75.54° (Fig. 8(b_1)), indicating that Cu-activated sphalerite also exhibits strong hydrophobicity. After adding IDS, the contact angle of Cu-activated sphalerite is only decreased by 1.69°, showing that only a trace of IDS was adsorbed on the surface of Cu-activated sphalerite. Further addition of EX increased the contact angle of Cu-activated sphalerite to 80.75° (Fig. 8(b_3)). Therefore, IDS did not affect the adsorption of EX on the surface of Cu-activated sphalerite. Based on surface wettability analysis, IDS enhances the hydrophilicity of the pyrite surface. Moreover, IDS affects the adsorption of EX on the Cu-activated pyrite surface. Hereby, IDS can selectively separate sphalerite from pyrite in the EX−Cu system.

3.3 Reagent adsorption

The adsorption ability of the collector on the mineral surface determines the floatability of the mineral during flotation [30,31]. The adsorption ability of EX on the mineral surface was studied under different IDS dosages. Figure 9 shows the standard curve of the absorbance−EX concentration, with a high fitting index (R^2) of 0.99903. Therefore, using this curve to calculate the concentration of EX has high accuracy.

As shown in Fig. 10, as the dosage of IDS increased from 0 to 300 mg/L, the adsorption capacity of EX sharply decreased from 1.92×10^{-7} to 0.39×10^{-7} mol/g on the Cu-activated pyrite surface. The abovementioned analysis indicates that IDS aims to inhibit pyrite flotation by affecting EX adsorption on the Cu-activated pyrite surface. For sphalerite, when the dosage of IDS reached 400 mg/L, the adsorption capacity of EX on the surface of Cu-activated sphalerite remained above 1.5×10^{-7} mol/g, indicating that IDS has little effect on the adsorption of EX on the surface of Cu-activated sphalerite. This result is consistent with the abovementioned surface wettability analysis. Reagent adsorption analysis showed that the presence of IDS causes a difference in the adsorption of EX on the surfaces of Cu-activated pyrite and sphalerite. IDS inhibits the flotation of pyrite and allows the separation of sphalerite from pyrite in the EX−Cu(II) system.

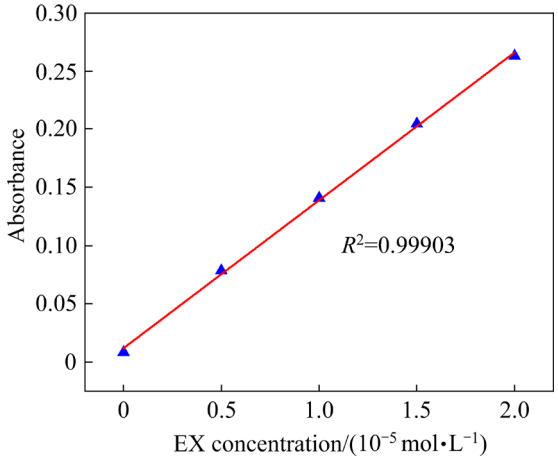

Fig. 9 Standard curve of EX adsorption

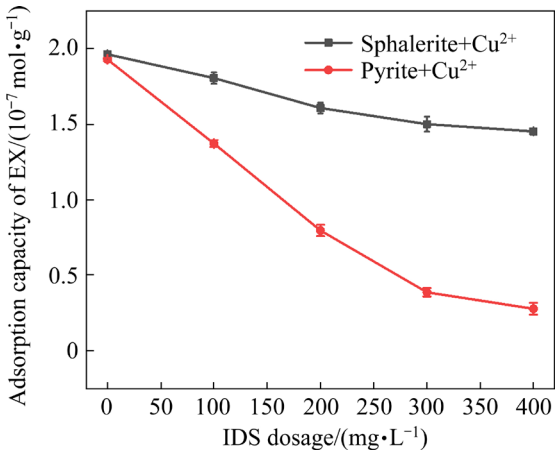

Fig. 10 Adsorption capacity of EX

3.4 LEIS analysis results

The adsorption of reagents can induce electrochemical reactions on the mineral surface. The interaction intensity between reagents and the mineral surface can be reflected by monitoring the conductivity of the mineral [30−33]. Surface wettability and reagent adsorption tests show that IDS can be adsorbed onto the pyrite surface and block the adsorption of EX on the pyrite surface in the EX−Cu(II) system. LEIS tests were conducted to investigate the changes in the surface electric properties of pyrite. The influence of IDS on the surface reactivity and flotation response of pyrite was characterized.

Figure 11(a) shows the LEIS map of pyrite. The uniform distribution of small red peaks indicates that the conductivity of the pyrite surface is relatively uniform, proving that there are fewer impurities in pyrite. Its average electrochemical impedance value is 273540.29 Ω. Figure 11(b) illustrates the LEIS map of pyrite after treatment

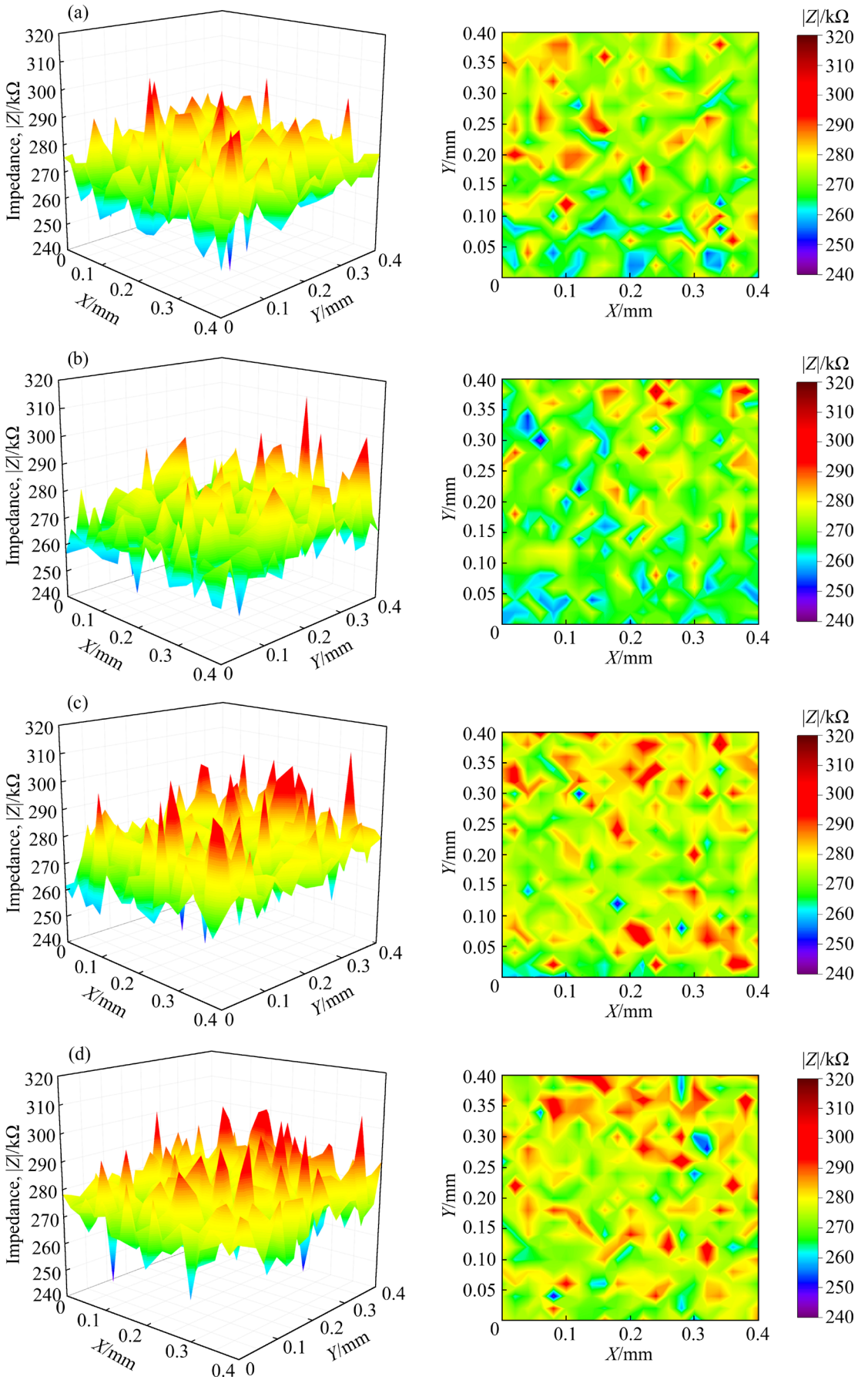

Fig. 11 LEIS results of pyrite: (a) Original pyrite; (b) Pyrite+Cu^{2+}; (c) Pyrite+Cu^{2+}+IDS; (d) Pyrite+Cu^{2+}+IDS+EX

with Cu^{2+}. The figure shows that the red peaks are significantly reduced, and the distribution of the peaks becomes uneven. The average electrochemical impedance value decreased to 270396.87 Ω, a difference of 3143.42 Ω compared with untreated pyrite. The abovementioned analysis indicated that Cu^{2+} can react with the pyrite surface, and the red peaks shown in Fig. 11(b) decrease because of the superior conductivity of Cu^{2+}. In addition, the average electrochemical impedance value decreases. LEIS tests were performed on Cu-activated pyrite treated with IDS (Fig. 11(c)). As shown in the figure, a large number of densely distributed red peaks appear, which are evenly distributed. This occurrence is primarily due to the uniform adsorption of IDS on the active sites of the pyrite surface. Its average electrochemical impedance value reaches 276663.31 Ω, an increase of 6266.44 Ω compared with that when only Cu^{2+} was added. This result is due to the chelation of IDS on the mineral surface, which increases the surface impedance of pyrite and reduces its reactivity.

Figure 11(d) shows the LEIS map of pyrite after adding EX, with an average electrochemical impedance value of 276985.46 Ω. Before and after the addition of EX, the density and distribution of red peaks in the LEIS map are almost identical, and the average impedance value is only increased by 322.15 Ω. This result indicates that IDS hinders the adsorption of EX on the pyrite surface. Therefore, IDS can change the electrochemical properties of the pyrite surface, thereby reducing the response rate and reactivity of pyrite flotation in the EX−Cu(II) system, which is consistent with the results of flotation experiments, surface wetting analysis, and adsorption tests.

3.5 Characterization results of surface adsorbed substances

FTIR analysis was performed to investigate the adsorbed substances of IDS on mineral surfaces and the effect of IDS on the adsorption of EX. FTIR is an intuitive and widely used method for studying the chemical adsorption of reagents on mineral surfaces [34,35]. Figure 12 shows the infrared spectra of EX and IDS. Figures 13(a) and (b) show the infrared spectra of pyrite and sphalerite before and after the adsorption of reagents, respectively. In the infrared spectrum of EX, the bands at 2975 and 2887 cm^{-1} are attributed to the stretching vibrations of —CH_3 and —CH_2, respectively [36,37]. The band at 1112 cm^{-1} is attributed to the stretching vibration of C—O—C [38,39]. The strong band at 1049 cm^{-1} is attributed to the stretching vibration of C═S [40]. In the infrared spectrum of IDS, the band at 2358 cm^{-1} is primarily attributed to the stretching vibration of —CH_2. The bands at 1569 and 1398 cm^{-1} are attributed to the stretching vibrations of —COO— and C—N, respectively [41−43].

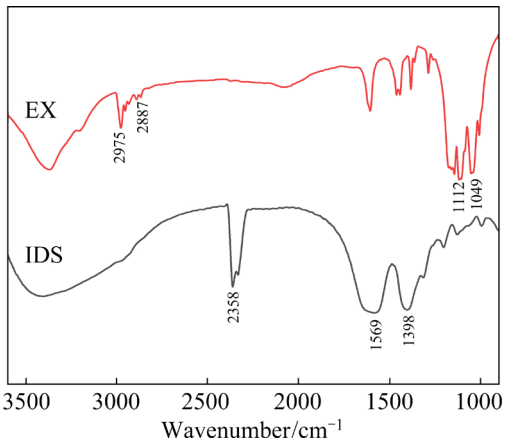

Fig. 12 FTIR spectra of EX and IDS

Figure 13(a) shows no characteristic peaks in the infrared spectrum of pyrite after Cu^{2+} activation. After treatment with IDS, two new absorption peaks appear in the infrared spectrum of pyrite, located at 2312 and 1535 cm^{-1}. The appearance of these two peaks is attributed to the —CH_2 and —COO— groups of IDS, with peak shifts of 46 and 34 cm^{-1}, respectively. This finding indicates that IDS interacts with the pyrite surface through chemical adsorption. After adding EX, no new characteristic peak appears on the pyrite surface. Therefore, IDS hinders the reaction of EX with the mineral surface.

As shown in Fig. 13(b), no characteristic peak of IDS was found in the infrared spectrum of the Cu-activated sphalerite surface after adding IDS. However, after adding EX, three new absorption peaks appear in the infrared spectrum of sphalerite, located at 2984 and 1057 cm^{-1}. Compared with the EX, the displacement distances are 9, 7, and 8 cm^{-1}. In the presence of IDS, EX can still interact with the surface of Cu-activated sphalerite through chemical adsorption. The abovementioned analysis indicates that the —COO— group in IDS interacts with the surface of Cu-activated pyrite through

chemical adsorption and impedes the adsorption of EX. By contrast, IDS exhibits weaker adsorption capacity on the surface of Cu-activated sphalerite, thereby ensuring the collecting performance of EX on Cu-activated sphalerite.

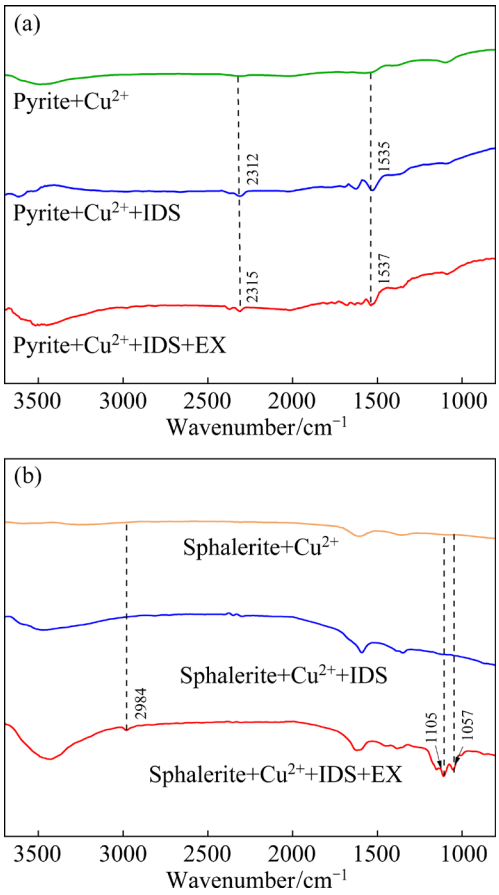

Fig. 13 FTIR spectra of minerals: (a) Pyrite; (b) Sphalerite

3.6 Surface properties

The flotation tests, surface wettability, reagent adsorption capacity, LEIS, and FTIR analyses demonstrate that IDS can alter the physicochemical properties of pyrite surfaces in the EX−Cu(II) system. In addition, IDS can selectively separate sphalerite from pyrite. In this section, XPS analysis was conducted to quantify and detect the elemental states on mineral surfaces, providing clear analysis of the differences in the binding sites and adsorption mechanisms of IDS on pyrite and sphalerite surfaces.

3.6.1 XPS full-spectra

The XPS full-spectra of the pyrite before and after treatment with the reagents are shown in Fig. 14, and the corresponding element contents are listed in Table 2. The spectrum of the pyrite surface treated with Cu^{2+} (Fig. 14(a)) showed binding energy peaks of C, O, S, Fe, and Cu, accounting for 34.73%, 18.78%, 34.79%, 8.55%, and 3.15% (in molar fraction, the same below), respectively. After adding IDS (Fig. 14(b)), the contents of C and O on the pyrite surface increased to 44.76% and 21.93%, respectively, and a new element N appeared with a content of 1.10%. Simultaneously, the content of Cu decreased from 3.15% to 0.80%. Therefore, IDS can be adsorbed onto the pyrite surface through the —COO— and N-centered active groups, and the adsorption of IDS harms Cu^{2+} on the pyrite surface. Upon further addition of EX (Fig. 14(d)), the contents of C, O, S, N, Fe, and Cu on the pyrite surface accounted for 42.80%, 23.43%, 23.72%, 1.33%, 8.00%, and 0.72%, respectively, showing only slight changes compared with the case when IDS was added alone. When only EX was added (Fig. 14(c)), the contents of C, O, S, Fe, and Cu changed to 68.82%, 17.46%, 9.34%, 2.92%, and 1.46%, respectively. Therefore, EX can be adsorbed onto the Cu-activated pyrite surface in the absence of IDS, but the presence of IDS hinders such adsorption.

The XPS full-spectra and corresponding element compositions of sphalerite before and after reagent treatment are shown in Fig. 15 and Table 3, respectively. After the action of Cu^{2+} on the surface of sphalerite, the binding energy peaks of C (64.99%), O (19.94%), S (9.45%), N (0.65%), Zn (2.35%), and Cu (2.62%) were detected (Fig. 15(a)). The presence of N was primarily attributed to environmental contamination. After the addition of IDS (Fig. 15(b)), the contents of C, O, S, N, Zn, and Cu on the surface of sphalerite changed to 67.62%, 15.50%, 9.77%, 0.79%, 4.56%, and 1.76%, respectively. The changes were relatively small compared with the case without IDS, indicating that IDS had little adsorption on the surface of sphalerite after Cu^{2+} activation. After the subsequent addition of EX in the presence of IDS (Fig. 15(d)), the surface elemental content of sphalerite changed significantly, with C content decreasing to 42.58% and S and Zn increasing to 24.21% and 13.46%, respectively. Meanwhile, in the presence of EX, the types and contents of surface elements of sphalerite were the same with or without IDS. These results demonstrate that the presence of IDS does not significantly affect the adsorption of EX on the surface of Cu-activated sphalerite.

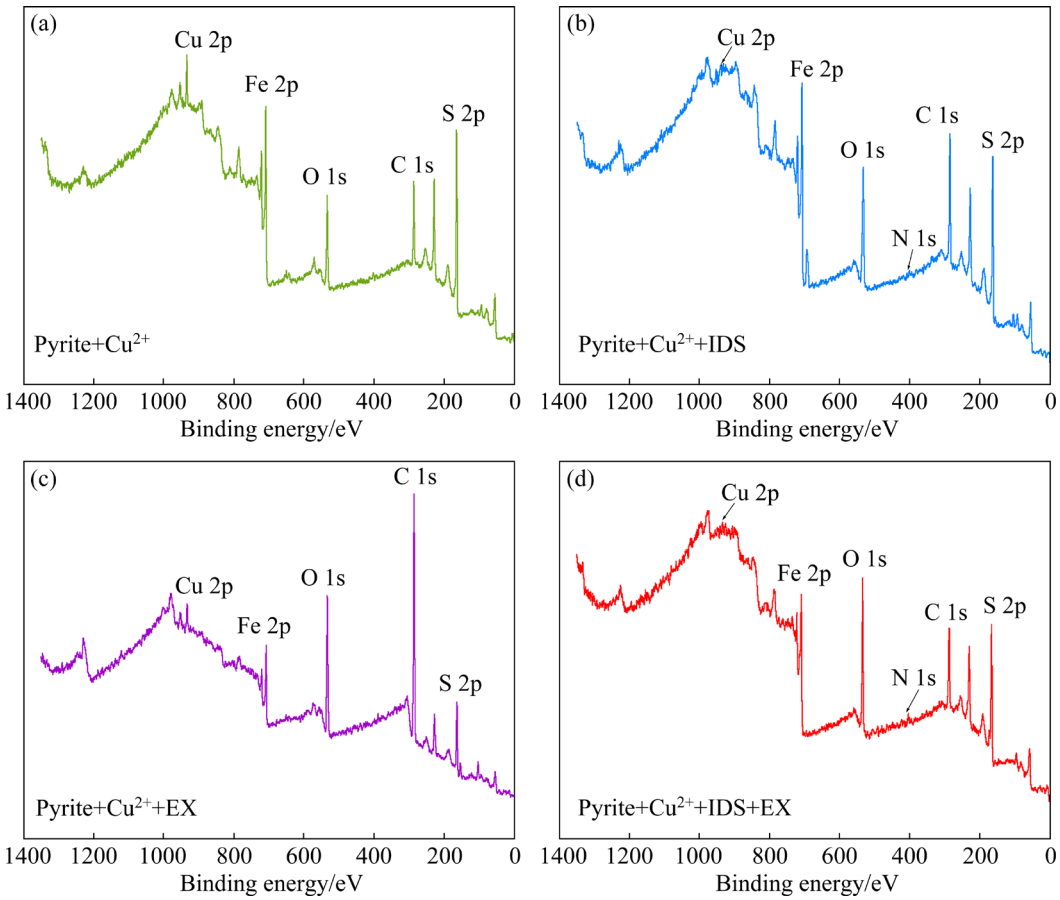

Fig. 14 XPS full-spectra of pyrite

Table 2 Elemental contents of pyrite (at.%)

Sample	C	O	S	N	Fe	Cu
Pyrite+Cu^{2+}	34.73	18.78	34.79	–	8.55	3.15
Pyrite+Cu^{2+}+IDS	44.76	21.93	24.41	1.10	7.00	0.80
Pyrite+Cu^{2+}+EX	68.82	17.46	9.34	–	2.92	1.46
Pyrite+Cu^{2+}+IDS+EX	42.80	23.43	23.72	1.33	8.00	0.72

XPS full-spectrum and element content analysis showed significant differences in the adsorption behavior of IDS on the surfaces of pyrite and sphalerite in the EX−Cu(II) system. This condition is necessary for achieving selective inhibition of pyrite by IDS. IDS may have achieved separation through two methods: First, IDS is adsorbed onto the pyrite surface via —COO— and N-centered active groups, occupying the adsorption site; Second, the addition of IDS can make the Cu^{2+} fall off on the pyrite surface, which affects the collection ability of EX.

3.6.2 XPS fine-spectrum analysis

Fine-spectrum analysis was conducted to confirm the conclusions obtained from the XPS full-spectrum and corresponding element content analysis. As shown in Fig. 16(a), the O 1s spectrum of pyrite clearly shows three binding peaks at 530.04, 531.69, and 533.21 eV after the action of Cu^{2+}, which can be attributed to metal oxides, metal hydroxides, and adsorbed water, respectively [44]. After the addition of IDS, a new binding peak appeared at 532.70 eV in the O 1s spectrum of pyrite, which can be attributed to the C=O/O—C=O groups [45]. The appearance of the new binding peak indicates that IDS is adsorbed onto the surface of pyrite through the —COO— group. As shown in Fig. 16(b), the N 1s peak intensity on the surface

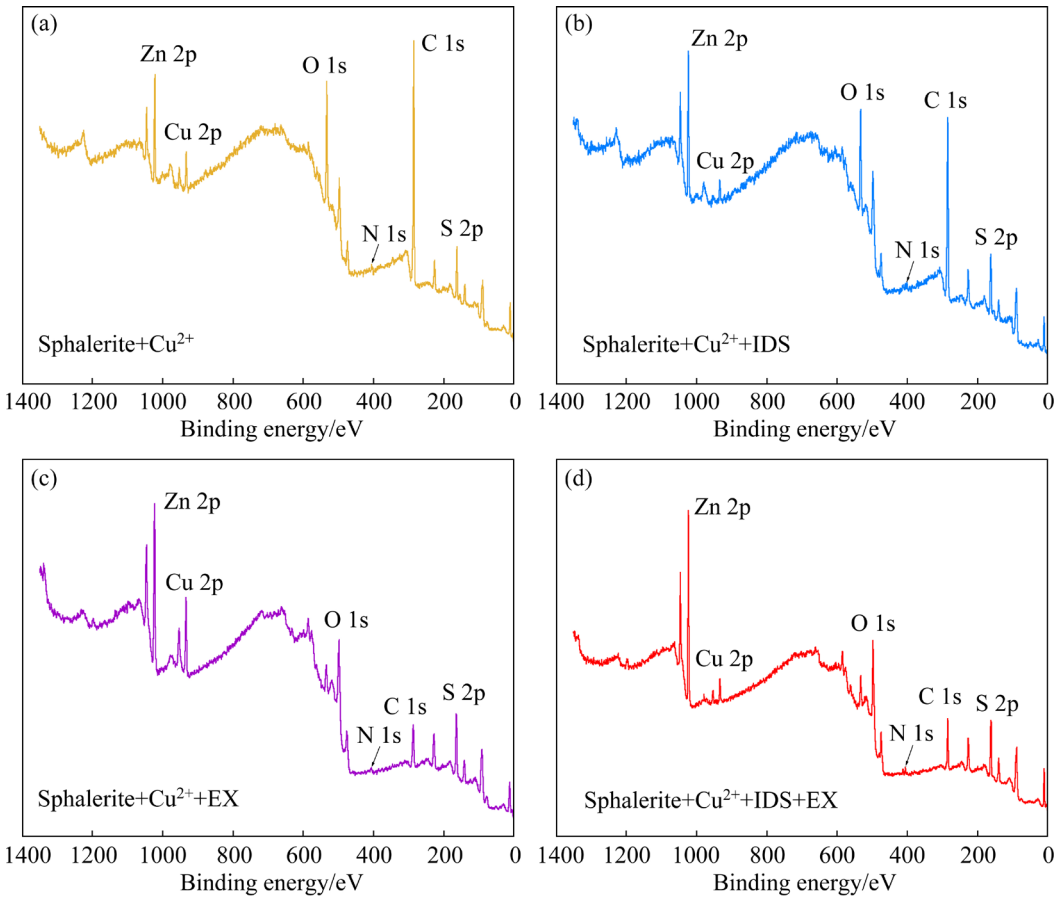

Fig. 15 XPS full-spectra of sphalerite

Table 3 Elemental contents of sphalerite (at.%)

Sample	C	O	S	N	Zn	Cu
Sphalerite+Cu^{2+}	64.99	19.94	9.45	0.65	2.35	2.62
Sphalerite +Cu^{2+}+IDS	67.62	15.50	9.77	0.79	4.56	1.76
Sphalerite +Cu^{2+}+EX	42.77	11.81	26.94	0.86	13.26	4.36
Sphalerite +Cu^{2+}+IDS+EX	42.58	14.56	24.21	0.98	13.46	4.21

of pyrite is very weak after the action of Cu^{2+}, indicating that no N is detected on the surface of pyrite, which is consistent with the abovementioned analysis results of the full-spectrum and element content. After IDS treatment, three binding peaks appeared at 398.81, 400.09, and 401.81 eV, which can be attributed to the —C—N—, —NH, and —NH—C—C═O groups, respectively [46]. This result further confirms that the N-centered active group in IDS can act on the surface of pyrite in the form of chemical adsorption.

As shown in Fig. 16(c), the spectrum indicates that the peak at 707.10 eV corresponds to the low-spin Fe^{2+} site in the pyrite lattice. The Fe(II)—S binding energy is located at 708.98 eV on the surface, while the binding energies at 710.40 and 711.50 eV are attributed to Fe(III)−O/OH, which are related to the oxides and hydroxides of Fe^{3+}, respectively [35,47,48]. After IDS treatment, a new peak appears at a binding energy of 709.78 eV, which may be due to the chelation of —COO— or N-centered active groups on the IDS with Fe^{3+}. Figure 16(d) shows that the Cu $2p_{3/2}$ binding energy is located at 932.34 eV in the spectrum of pyrite surface after Cu^{2+} treatment, which is primarily attributed to Cu—S formed by Cu^{2+} and S of pyrite [49,50]. This result also confirms the adsorption of Cu^{2+} on the pyrite surface. However,

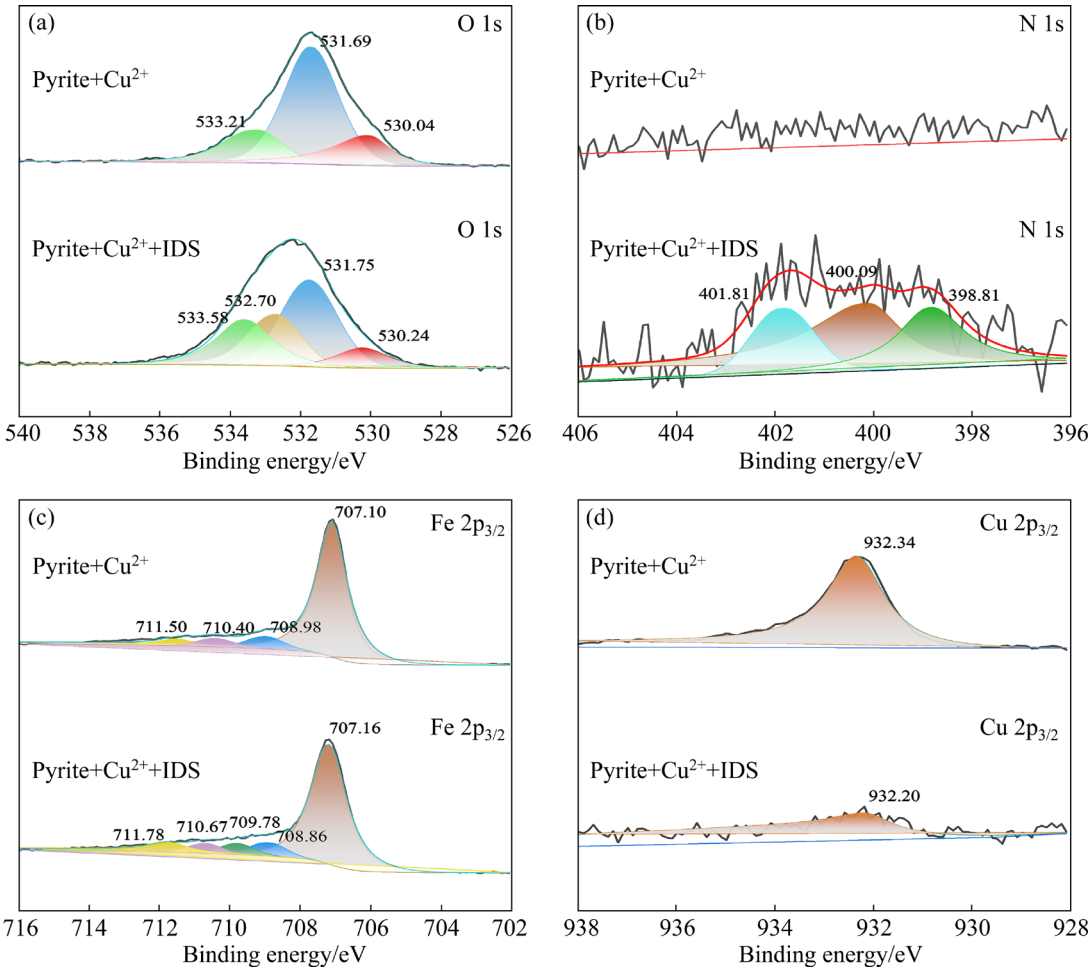

Fig. 16 XPS fine-spectra of pyrite

after IDS treatment, the intensity of the Cu—S peak is greatly weakened, which is consistent with the analysis of the relative element content (the content of Cu^{2+} on the pyrite surface decreases from 3.15% to 0.8%). This result further demonstrates the desorption effect of IDS on Cu^{2+} on the pyrite surface, affecting the collection ability of EX.

As shown in Fig. 17(a), the O 1s spectrum of sphalerite exhibits three binding energy peaks after the action of Cu^{2+}. The peak at 529.99 eV corresponds to the metal oxide on the sphalerite surface, the peak at 532.17 eV is attributed to the hydroxide on the surface, and the peak at 533.39 eV is attributed to O in the adsorbed water [51,52]. After IDS treatment, no new binding energy peak appears in the O 1s spectrum of sphalerite, and the original three peaks remain within a displacement range of 0.2 eV. Therefore, the —COO— group in IDS is not adsorbed onto the sphalerite surface. Figure 17(b) shows that a binding energy peak appears at 405.06 eV in the N 1s spectrum of sphalerite after treatment with Cu^{2+} primarily because of N contamination in the sample environment. After IDS treatment, a binding energy peak of N 1s still appears at 405.76 eV. Considering that the characteristic peak of N 1s is located in the range of 398−402 eV in IDS [46], the binding energy peak at 405.76 eV does not belong to IDS, indicating that the N-centered functional group in IDS cannot be adsorbed onto the surface of sphalerite.

As shown in Fig. 17(c), the peak in the Cu $2p_{3/2}$ spectrum of Cu-activated sphalerite is located at 932.79 eV. This peak is primarily attributed to the substitution of Cu^{2+} for Zn on the sphalerite surface, forming Cu—S bonds. Upon the addition of IDS, the peak of Cu $2p_{3/2}$ in the sphalerite spectrum changes to 932.47 eV, exhibiting only a minimal shift of 0.32 eV compared with the case when IDS is not added,

which falls within the range of the testing error. The abovementioned observations indicate that IDS faces challenges in desorbing Cu^{2+} adsorbed onto the surface of sphalerite, thereby failing to influence the capturing efficiency of EX. This result further underscores the ability of IDS to precisely separate sphalerite from pyrite in the EX−Cu(II) system.

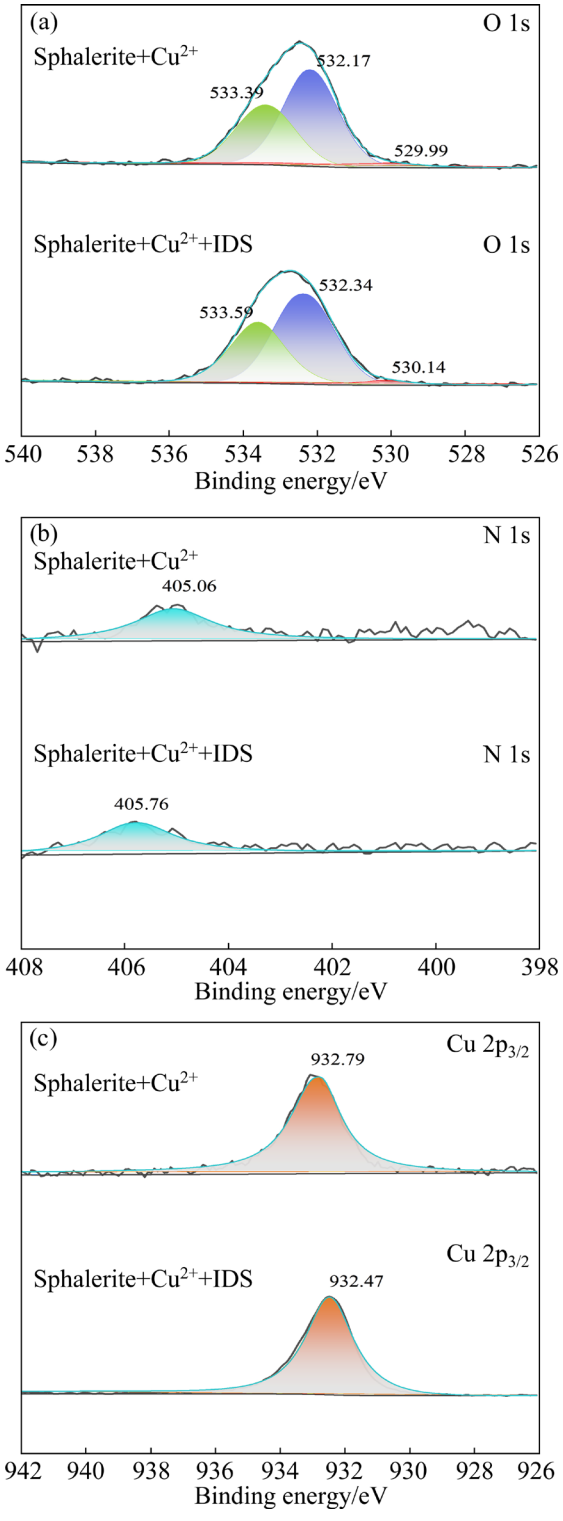

Fig. 17 XPS fine-spectra of sphalerite

4 Conclusions

(1) The flotation tests demonstrate that IDS can effectively separate sphalerite and pyrite under low alkaline conditions. Furthermore, high-quality zinc concentrates with a Zn grade of 58.48% and a recovery of 91.24% through mixed mineral flotation have been obtained.

(2) Surface wettability tests, reagent adsorption tests, and LEIS analysis have demonstrated that IDS can selectively adsorb onto the surface of Cu-activated pyrite, causing alterations in its physicochemical properties. The presence of IDS severely hampers the adsorption of EX on the Cu-activated pyrite surface. Consequently, IDS reduces the response rate and reactivity of pyrite flotation in the EX−Cu(II) system.

(3) FTIR and XPS analyses have revealed that IDS acts on the surface of Cu-activated pyrite through chemical adsorption, primarily through the complexation of its —COO— groups and N-centered active groups with the formation of iron ions on the pyrite surface. Introducing IDS leads to the detachment of copper ions from the Cu-activated pyrite surface. By contrast, IDS exhibits weaker adhesion on the surface of Cu-activated sphalerite, causing it to be easily displaced by EX through competitive adsorption.

CRediT authorship contribution statement

Wen-chao DONG: Data curation, Formal analysis, Investigation, Methodology, Software, Visualization, Writing − Original draft, Review & editing; **Run-qing LIU:** Formal analysis, Investigation, Methodology, Visualization, Writing − Review & editing; **Chang-tao WANG:** Conceptualization, Data curation, Formal analysis, Funding acquisition, Investigation, Methodology, Project administration, Resources, Supervision, Validation, Writing − Review & editing; **Zheng-qiang CAO:** Conceptualization, Investigation, Methodology, Project administration, Resources, Supervision, Validation, Writing − Review & editing; **Wei SUN:** Conceptualization, Formal analysis, Funding acquisition, Investigation, Methodology, Project administration.

Declaration of competing interest

The authors declare that they have no known competing financial interests or personal relationships that could have appeared to influence the work reported

in this paper.

Acknowledgments

The authors would like to thank financial supports from the National Natural Science Foundation of China (No. 52174272), the Fundamental Research Funds for the Central Universities of Central South University, China (No. 2021zzts0306), and the Hunan Provincial Natural Science Foundation of China (No. 2020JJ5736).

References

[1] LUO Zhong-tao, GUO Jin-yang, LIU Xiao-hai, MU Yuan-dong, ZHANG Mei-xiang, ZHANG Meng, TIAN Chong-fei, OU Jia-hui, MI Jie. Preparation of ceramsite from lead−zinc tailings and coal gangue: Physical properties and solidification of heavy metals [J]. Construction and Building Materials, 2023, 368: 130426.

[2] KAMAL ARIFFIN N I, MAMAT M H, KAMARUZAMAN D, ABDULLAH M H, PARIMON N, YAAKOB M K, MALEK M F, VASIMALAI N, SURIANI A B, MOHAMED A, AHMAD M K, RUSOP M. Metal-doped zinc oxide nanostructures for nanogenerator applications: A review [J]. Materials Today: Proceedings, 2023, 75: 51−57.

[3] QIU Ting-sheng, LI Guo-dong, LI Xiao-bo, YAN Hua-shan, LIU Chen. Influence of high concentration Zn^{2+} on floatability of sphalerite in acidic system [J]. Transactions of Nonferrous Metals Society of China, 2021, 31: 2128−2138.

[4] SELÇUK Ö, AÇIKBAŞ G, NURCAN Ç A. Induced superhydrophobic and antimicrobial character of zinc metal modified ceramic wall tile surfaces [J]. Applied Surface Science, 2018, 438: 136−146.

[5] CUI Yan-fang, JIAO Fen, QIN Wen-qing, DONG Liu-yang, WANG Xu. Synergistic depression mechanism of zinc sulfate and sodium dimethyl dithiocarbamate on sphalerite in Pb−Zn flotation system [J]. Transactions of Nonferrous Metals Society of China, 2020, 30: 2547−2555.

[6] WEI Qian, JIAO Fen, DONG Liu-yang, LIU Xue-duan, QIN Wen-qing. Selective depression of copper-activated sphalerite by polyaspartic acid during chalcopyrite flotation [J]. Transactions of Nonferrous Metals Society of China, 2021, 31: 1784−1795.

[7] ZHANG Zhi-yong, LIU Sheng, LIU Feng-yue, MOHAMED AHMED M M, QU Xiao-yan, LIU Guang-yi. The flotation separation of sphalerite from pyrite through a novel flotation reagent system of $FeCl_3$−$CuSO_4$−aminotriazolethione [J]. Journal of Molecular Liquids, 2022, 345: 116997.

[8] ZHANG Li-min, GAO Jian-de, KHOSO S A, LIU Yu-ling, TIAN Meng-jie. Interaction mechanism of the adopted reagents in the flotation recovery of sphalerite and pyrite from a galena flotation tailing: First-principles calculations [J]. Colloids and Surfaces A: Physicochemical and Engineering Aspects, 2021, 617: 126378.

[9] WEI Qian, DONG Liu-yang, JIAO Fen, QIN Wen-qing, PAN Zu-chao, CUI Yan-fang. The synergistic depression of lime and sodium humate on the flotation separation of sphalerite from pyrite [J]. Minerals Engineering, 2021, 163: 106779.

[10] CAO Zhao, WANG Peng, ZHANG Wen-bo, ZENG Xiao-bo, CAO Yong-dan. Mechanism of sodium sulfide on flotation of cyanide-depressed pyrite [J]. Transactions of Nonferrous Metals Society of China, 2020, 30: 484−491.

[11] SUN Xin, HUANG Ling-yun, WU Dan-dan, TONG Xiong, YANG Si-yuan, HU Bo. The selective depression effect of dextrin on pyrite during the Zn−Fe sulfides flotation under low alkaline conditions [J]. Colloids and Surfaces A: Physicochemical and Engineering Aspects, 2022, 650: 129573.

[12] HAO Jia-mei, LIU Jian, YU Yun-long, GAO Hu-lin, QIN Xiao-yan, BAI Xu. Depressants for separation of chalcopyrite and molybdenite: Review and prospects [J]. Minerals Engineering, 2023, 201: 108209.

[13] QIN Wen-qing, WANG Xing-jie, MA Li-yuan, JIAO Fen, LIU Rui-zeng, GAO Ke. Effects of galvanic interaction between galena and pyrite on their flotation in the presence of butyl xanthate [J]. Transactions of Nonferrous Metals Society of China, 2015, 25: 3111−3118.

[14] DING Zhan, BI Yun-xiao, LI Jie, YUAN Jia-qiao, DAI Hui-xin, BAI Shao-jun. Flotation separation of chalcopyrite and pyrite via Fenton oxidation modification in a low alkaline acid mine drainage (AMD) system [J]. Minerals Engineering, 2022, 187: 107818.

[15] WANG Chang-tao, LIU Run-qing, ZHAI Qi-lin, XIE Zhen-hui, SUN Wei, LI Pei-yuan, WANG Zhou-he. Exploring the effect of pulp aeration and lime-aid grinding on pyrrhotite-rich type copper sulfide ore flotation separation [J]. Separation and Purification Technology, 2023, 311: 123268.

[16] WANG Chang-tao, LIU Run-qing, AHMED KHOSO S, LU Hong-yu, SUN Wei, NI Zhang-yuan, LYU Fei. Combined inhibitory effect of calcium hypochlorite and dextrin on flotation behavior of pyrite and galena sulphides [J]. Minerals Engineering, 2020, 150: 106274.

[17] PAN Zu-chao, LIU Zhi-cheng, XIONG Jing-jing, LI Jia-lei, WEI Qian, ZHANG Zheng-quan, JIAO Fen, QIN Wen-qing. Application and depression mechanism of sodium sulfite on galena−pyrite mixed concentrate flotation separation: Huize Lead−Zinc Mine, China, as an example [J]. Minerals Engineering, 2022, 185: 107696.

[18] MU Yu-fan, PENG Yong-jun. The role of sodium metabisulphite in depressing pyrite in chalcopyrite flotation using saline water [J]. Minerals Engineering, 2019, 142: 105921.

[19] KHOSO S A, HU Yue-hua, LÜ Fei, GAO Ya, LIU Run-qing, SUN Wei. Xanthate interaction and flotation separation of H_2O_2-treated chalcopyrite and pyrite [J]. Transactions of Nonferrous Metals Society of China, 2019, 29: 2604−2614.

[20] CAO Zhao, CHEN Xu-meng, PENG Yong-jun. The role of sodium sulfide in the flotation of pyrite depressed in chalcopyrite flotation [J]. Minerals Engineering, 2018, 119: 93−98.

[21] LÓPEZ VALDIVIESO A, CELEDÓN CERVANTES T, SONG S, ROBLEDO CABRERA A, LASKOWSKI J S. Dextrin as a non-toxic depressant for pyrite in flotation with xanthates as collector [J]. Minerals Engineering, 2004, 17: 1001−1006.

[22] FLETCHER B, CHIMONYO W, PENG Yong-jun. A comparison of native starch, oxidized starch and CMC as copper-activated pyrite depressants [J]. Minerals Engineering, 2020, 156: 106532.

[23] MONYAKE K C, ALAGHA L. Enhanced separation of base metal sulfides in flotation systems using chitosan-grafted-polyacrylamides [J]. Separation and Purification Technology, 2022, 281: 119818.

[24] ZHENG Ming-yu, PENG Tie-feng, WANG Yan-hong, LUO Li-qun, SHAO Wei, GAO Jia-qi, LU Qi. Flotability of galena and pyrite using 2-mercaptobenzimidazole as a chelating agent: Adsorption characteristics and flotation mechanisms [J]. Powder Technology, 2021, 393: 449−460.

[25] HAN Guang, WEN Shu-ming, WANG Han, FENG Qi-cheng. Interaction mechanism of tannic acid with pyrite surfaces and its response to flotation separation of chalcopyrite from pyrite in a low-alkaline medium [J]. Journal of Materials Research and Technology, 2020, 9: 4421−4430.

[26] HAN Guang, WEN Shu-ming, WANG Han, FENG Qi-cheng. Selective adsorption mechanism of salicylic acid on pyrite surfaces and its application in flotation separation of chalcopyrite from pyrite [J]. Separation and Purification Technology, 2020, 240: 116650.

[27] FENG Bo, ZHONG Chun-hui, ZHANG Liang-zhu, GUO Yu-tao, WANG Tao, HUANG Zhi-qiang. Effect of surface oxidation on the depression of sphalerite by locust bean gum [J]. Minerals Engineering, 2020, 146: 106142.

[28] WANG Wen-min, XIN Xing, LI Bing, HUANG Hai-ming, LIU Xiao-ning, SONG Lan, WU Xiao-feng, HUANG Yue-fei. Effect of organics on Cu and Cr in recovered struvite from synthetic swine wastewater [J]. Journal of Cleaner Production, 2022, 360: 132186.

[29] HODES J, SIELAFF P, METZ H, KESSLER-BECKER D, GASSENMEIER T, NEUBERT R H H. The role of chelating agents and amino acids in preventing free radical formation in bleaching systems [J]. Free Radical Biology and Medicine, 2018, 129: 194−201.

[30] BAI Xu, LIU Jian, WEN Shu-ming, WANG Yu, LIN Yi-lin. Effect of ammonium salt on the stability of surface sulfide layer of smithsonite and its flotation performance [J]. Applied Surface Science, 2020, 514: 145851.

[31] LIU Jian, WANG Yu, LUO De-qiang, CHEN Lu-zheng, DENG Jiu-shuai. Comparative study on the copper activation and xanthate adsorption on sphalerite and marmatite surfaces [J]. Applied Surface Science, 2018, 439: 263−271.

[32] DONG Wen-chao, LIU Run-qing, WANG Chang-tao, ZHU Xian-wen, XIE Zhen-hui, SUN Wei. Insight into selective depression of sodium thioglycallate on arsenopyrite flotation: Adsorption mechanism and constructure [J]. Journal of Molecular Liquids, 2023, 377: 121480.

[33] YU Li, LIU Quan-jun, LI Shi-mei, DENG Jiu-shuai, LUO Bin, LAI Hao. Depression mechanism involving Fe^{3+} during arsenopyrite flotation [J]. Separation and Purification Technology, 2019, 222: 109−116.

[34] LI Jia-lei, MA Yin-yu, LI Guang-li, LIU Zhi-cheng, NING Shuai, PEI Bin, LANG Zhao-you, LIU Rui-zeng, LIU Dian-wen. Depression mechanism of $ZnSO_4$ and Na_2CO_3 on talc flotation [J]. Transactions of Nonferrous Metals Society of China, 2023, 33: 1559−1571.

[35] RAN Jin-cheng, LI Yue-peng, ZHAO Xin-miao, JIANG Man, GAO En-xia. Utilization of soluble starch as the depressant to flotation separation of pyrite from arsenopyrite [J]. Separation and Purification Technology, 2023, 310: 123155.

[36] ZHONG Chun-hui, FENG Bo, CHEN Yuan-gan, GUO Meng-chi, WANG Hui-hui. Flotation separation of molybdenite and talc using tragacanth gum as depressant and potassium butyl xanthate as collector [J]. Transactions of Nonferrous Metals Society of China, 2021, 31: 3879−3890.

[37] ZHANG Qian, WANG Yi-jie, FENG Qi-cheng, WEN Shu-ming, ZHOU Yao-wen, NIE Wen-lin, LIU Jun-bo. Identification of sulfidization products formed on azurite surfaces and its correlations with xanthate adsorption and flotation [J]. Applied Surface Science, 2020, 511: 145594.

[38] LU Ji-wei, TONG Zhong-yun, YUAN Zhi-tao, LI Li-xia. Investigation on flotation separation of chalcopyrite from arsenopyrite with a novel collector: N-butoxycarbonyl-O-isobutyl thiocarbamate [J]. Minerals Engineering, 2019, 137: 118−123.

[39] ZHANG Song, XIAN Yong-jun, WEN Shu-ming, LIANG Guan-yu, GENG Qing. Contribution of ammonia in xanthates adsorption onto copper oxide mineral surface in high-alkaline solution. [J]. Applied Surface Science, 2023, 630: 157294.

[40] ZHAO Wen-juan, YANG Bin, YI Ya-hui, FENG Qi-cheng, LIU Dian-wen. Synergistic activation of smithsonite with copper−ammonium species for enhancing surface reactivity and xanthate adsorption [J]. International Journal of Mining Science and Technology, 2023, 33: 519−527.

[41] QI Jing, LIU Guang-yi, DONG Yan. Probing the hydrophobic mechanism of N-[(3-hydroxyamino)-propoxy]-N-octyl dithiocarbamate toward bastnaesite flotation by in situ AFM, FTIR and XPS [J]. Journal of Colloid and Interface Science, 2020, 572: 179−189.

[42] CHANG Qing, HAO Xue-kui, DUAN Li-li. Synthesis of crosslinked starch-graft-polyacrylamide-co-sodium xanthate and its performances in wastewater treatment [J]. Journal of Hazardous Materials, 2008, 159: 548−553.

[43] WANG Zhen, CAO Jun, WANG Li, XIAO Jun-hui, WANG Jin-ming. Selective depression of arsenopyrite with in situ generated nanoparticles in pyrite flotation [J]. Minerals Engineering, 2021, 173: 107223.

[44] LUO Yuan-jia, XIA Yu-qin, WANG Changt-ao, CHEN Jian-hua, OU Le-ming. Application of calcium lignosulphonate as an environmentally friendly depressant in the Cu−As separation by froth flotation at low alkalinity [J]. Journal of Cleaner Production, 2023, 406: 137073.

[45] ZHU Huan-yu, YANG Bing-qiao, MARTIN R, ZHANG Han-quan, HE Dong-sheng, LUO Hui-hua. Flotation separation of galena from sphalerite using hyaluronic acid (HA) as an environmental-friendly sphalerite depressant [J]. Minerals Engineering, 2022, 187: 107771.

[46] CHEN Yan-fei, ZHANG Guo-fan, SHI Qing, YANG Si-yuan, LIU De-zhi. Utilization of tetrasodium iminodisuccinate to eliminate the adverse effect of serpentine on the flotation of pyrite [J]. Minerals Engineering, 2020, 150: 106235.

[47] NIU Xiao-peng, CHEN Jian-hua, LI Yu-qiong, XIA Liu-yin, LI Li, SUN He-yun, RUAN Ren-man. Correlation of surface oxidation with xanthate adsorption and pyrite flotation [J].

Applied Surface Science, 2019, 495: 143411.
[48] OWUSU C, FORNASIERO D, ADDAI-MENSAH J, ZANIN M. Influence of pulp aeration on the flotation of chalcopyrite with xanthate in chalcopyrite/pyrite mixtures [J]. International Journal of Mineral Processing, 2015, 134: 50−57.
[49] ZHANG Xing-rong, LU Lu-lin, LUO An-ruo, XIONG Wei, CHEN Jian-hua. Interface adsorption of 5-amino-1,3,4-thiadiazole-2-thiol on chalcopyrite surface as flotation depressant in Cu/Mo separation [J]. Applied Surface Science, 2023, 611: 155703.
[50] YIN Zhi-gang, SUN Wei, HU Yue-hua, ZHANG Chen-hu, GUAN Qing-jun, LIU Run-qing, CHEN Pan, TIAN Meng-jie. Utilization of acetic acid-[(hydrazinylthioxomethyl)thio]-sodium as a novel selective depressant for chalcopyrite in the flotation separation of molybdenite [J]. Separation and Purification Technology, 2017, 179: 248−256.
[51] CHEN Yuang-an, FENG Bo, PENG Jin-xiu, WANG Zi-ming. Selective flotation of galena from sphalerite using a combination of $KMnO_4$ and carboxylated chitosan [J]. Applied Surface Science, 2022, 602: 154412.
[52] YANG Bing-qiao, ZHU Huan-yu, ZENG Long-yan, FENG Jin-chan, LUO Hui-hua. An environmental-friendly sphalerite depressant (2-Hydroxyphosphonoacetic Acid) for the selective flotation separation of sphalerite from galena [J]. Journal of Molecular Liquids, 2021, 343: 117614.

亲铁型抑制剂在 EX−Cu(II)体系中精确分离闪锌矿和黄铁矿的界面吸附和反应活性

董文超，刘润清，王长涛，曹正强，孙 伟

中南大学 资源加工与生物工程学院，长沙 410083

摘 要：以亚氨基二琥珀酸四钠(IDS)为抑制剂，在 EX−Cu(II)(乙基黄药和 Cu^{2+})体系中分离闪锌矿和黄铁矿。浮选试验结果表明，IDS 在弱碱性条件下可选择性分离闪锌矿和黄铁矿。通过混合矿物浮选，获得了锌品位为 58.48%、回收率为 91.24%的优质锌精矿。通过表面润湿性测试、吸附量测试、LEIS、FTIR 和 XPS 进行了机理研究。结果表明，IDS 阻止了 EX 在黄铁矿表面的吸附，从而降低了黄铁矿的响应性和反应活性。IDS 的引入导致 Cu^{2+}从铜活化的黄铁矿表面脱离，这为 IDS 提供了通过—COO—和以 N 原子为中心的活性基团与黄铁矿表面 Fe 位点螯合的机会。相比之下，IDS 在铜活化闪锌矿表面的附着力较弱，容易被 EX 通过竞争吸附取代。

关键词：界面吸附；反应活性；分离；闪锌矿；黄铁矿；亚氨基二琥珀酸四钠

(Edited by Wei-ping CHEN)